Sulfur and nitrogen-doped porous cobalt carbon catalyst for high efficient aerobic oxidation of hydrocarbons

Xiu Lin, Shanshan Jie, Zhigang Liu[*]

State Key Laboratory of Chemo/Biosensing and Chemometrics, School of Chemistry and Chemical Engineering, Hunan University, Changsha, 410082, Hunan, China

ARTICLE INFO

ABSTRACT

The selective oxidation of hydrocarbons to corresponding ketones under green reaction conditions is of more and more important in chemical processes due to environmental and economic pressure. In this respect, we successfully prepared high efficient sulfur and nitrogen-doped porous cobalt carbon catalyst through a simple but efficient one-pot method. Potassium thiocyanate (KSCN) is using as sulfur source and complexing agent, what's more, KSCN also acts as pore-forming agent to create larger specific surface area. In addition, the as-obtained catalyst shows high catalytic performance for oxidation of hydrocarbons under solvent-free and oxygen as oxidant conditions, especially for ethylbenzene, the conversion is up to 82% with 88% of selectivity for acetophenone, which is an exciting result due to the relative low activity of oxygen in comparison with tert-butyl hydroperoxide as oxidant. This is due to structure defect and Co_4S_3 by the doping of KSCN in CoNC catalysts, which may result in the improvement of the catalytic performance of the catalysts.

1. Introduction

The selective oxidation of hydrocarbons which has drawn great attention is one of the challenging and fundamental organic reactions in green chemistry since the main products of ketones are important intermediates and fine chemicals in perfume, pharmaceutical, cosmetics industries and so on [1,2]. Under the strict pressure of environmental regulation, researchers have developed many environmentally benign, low cost, and facile methods to reduce or end use of a massive glut of toxic and expensive stoichiometric metal oxidants [3]. Recently, an increasing effort has been made to replace those unsustainable technologies by using air or molecular oxygen (O_2) under solvent-free conditions [4–6]. For example, Xu et al. took advantage of a strong base-type catalyst to oxidize ethylbenzene to corresponding acetophenone using O_2 as oxidant under mild reaction conditions, which exhibited about 29% of conversion and 71% of selectivity [7]. However, Ma et al. reported that ethylbenzene was almost completely converted to acetophenone with tert-butyl hydroperoxide (TBHP) as oxidant under water solvent and the help of N-doped graphitic catalysts [8]. Thus, the most challenging part for O_2 remains limited catalytic performance compared to other liquid-phase processes. The development of efficient green catalyst would have a significant impact on the process of aerobic oxidation under solvent-free condition.

Recent studies have demonstrated that nitrogen doped metal carbon materials (MNC) have attracted considerable attention due to their pronounced catalytic performance, which is likely to result from metal coordinated with nitrogen to generate M–N active sites [9–11]. MNC have been widely researched and show excellent catalytic performance whether in heterogeneous catalysis, electrocatalysis or photocatalysis [11–15]. Scientists have put their attention to other heteroatoms (e.g., B, S, P and I) based on MCN [16–19]. It is an effective strategy that the introduction of heteroatoms into carbon frameworks for improving its catalytic performance, arising from the variations in charge and spin densities of carbon atoms adjacent to doped heteroatoms, as demonstrated by theoretical calculation and experimental studies [8,17,20]. Sulfur and nitrogen-doped carbon catalysts have performed excellent performance in electrocatalysis and batteries, which maybe ascribe to active sites surrounded by sulfur species [19]. As far as we know, however, sulfur and nitrogen-doped carbon catalysts are seldom applied into heterogeneous catalysis. Due to the presence of extensive studies for nitrogen doped carbon based catalysts with or without metals [5,8,21], sulfur atom which properties (defect, synergistic effect, charge transfer, etc.) are similar to nitrogen atom is recognized as a novel and efficient doped atom for heterogeneous catalysis. Thus, developing cheap and effective sulfur and nitrogen-doped carbon catalysts is promising and necessary to enhance catalytic efficiency of heterogeneous catalysis.

KSCN is widely used as poisoning agent in catalysis due to its strong complexing ability for transition metal ions. Meanwhile, KSCN is a good dopant to prepare catalyst containing nitrogen and sulfur elements

---

because of its excellent characteristics of rich nitrogen and sulfur as well as strong complexing ability [22]. Herein, we report one-pot method to successfully prepare sulfur and nitrogen-doped porous cobalt carbon catalyst (S–CoNC), in which 1,10-phenanthroline is used as carbon and nitrogen source and KSCN is mainly using as sulfur source and pore-forming agent. The high specific surface area of S–CoNC is produced under the assistance of KSCN and significantly higher than carbon based materials synthesized by pyrolyzing directly 1,10-phenanthroline with other special pore-forming agent or support. In comparison with the reported catalysts for aerobic oxidation of saturated hydrocarbons, the novel S–CoNC exhibited significantly higher catalytic performance, and the catalytic active site is studied in detail.

2. Materials and methods

2.1. Materials and reagents

1,10-Phenanthroline (99.0%), KSCN (98.0%), cobalt nitrate hexahydrate (99.0%), mercapto acetic acid (MMA) (98.0%) and all solvents were of commercially available analytical reagent and used without further purification.

2.2. Catalyst preparation

1 mmol of cobalt nitrate hexahydrate and 2 mmol of 1,10-phenanthroline were dissolved into 30 mL of absolute ethanol by sonication. The mixed solution was stirred at 60 °C for 0.5 h, in which a large amount of yellow precipitation was formed at the beginning. After that, 3 mmol of KSCN was quickly added into this mixture, and then continue to stir at the same temperature for 2 h. It is remarkable that the precipitation quickly changed from yellow to pink in few seconds after the addition of KSCN. The mixture was cooled down to room temperature after stirring 2 h and suction filtration. During the process of materials preparation, the following reactions could occur [23]:

$$Co^{2+} + 2 \, Phen = Co(Phen)_2^{2+}$$

$$Co(Phen)_2^{2+} + 2 \, SCN_- = Co(Phen)_2(SCN)_2$$
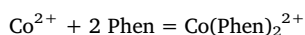
The pink precipitate was washed for several times by absolute ethanol and dried at 80 °C for overnight. The obtained product (69% of yield calculated from the mass ratio of obtained to added) was grinded and transferred to crucible, and then pyrolysis was conducted at 800 °C under N_2 for 2 h at the heating rate of 3 °C/min. The final catalyst was collected by grinding, denoted as S–CoNC.

For the control groups, S–CoNC-700 and S–CoNC-900 were only changed pyrolysis temperature; CoNC and S–CoNCm were prepared at the same procedure except for the addition of KSCN and mercapto acetic acid (MMA) as S source, respectively; S–CoNC was treated with HCl solution at 80 °C for 4 h and then S–CN was synthesized.

2.3. Characterizations

Structure and morphology characterization: The morphology and structure of catalyst were investigated by field emission scanning electronic microscopy (SEM, JSM-6700F microscope) and transmission electron microscopy (TEM, Tecnai G2 F20 S-TWIN instrument). The structure and phase purity of catalyst were examined by X-ray diffraction (XRD, Japan XRD-6100 diffractometer) equipped with Ni-filtered Cu Kα radiation (50 kV, 10 mA). Raman spectrum was recorded with LabRAM Aramis micro Raman spectrometer (laser wavelength 633 nm) using a 50× optical objective with an average spot size of around 2 μm. Nitrogen adsorption–desorption isotherms were obtained on Quantachrome NOVA-1000e at 77 K. Prior to the measurement, the samples were degassed at 200 °C for 3 h with a gas flow of N_2. The surface composition and oxidation state of catalyst were further investigated by X-ray photoelectron spectroscopy (XPS) on PHI 5000C

ESCA system (PerkinElmer) with an Al Kα (1486.6 eV) X-ray source, and all binding energies were referred to the C 1s peak (284.5 eV) arising from the C−C bonds.

2.4. Catalytic performance test

The selective aerobic oxidation of hydrocarbons was carried out in Teflon stainless steel autoclave, in which the ethylbenzene oxidation is the model reaction. In this process, 82 mmol of substrate and 30 mg of catalyst were added in reactor, which was sealed and filled with 0.8 MPa of O_2 then kept at 120 °C for 5 h with continuous magnetic stirring. The reacted solution was separated through centrifugation, meanwhile the catalyst was collected and washed for 3 times with absolute ethanol, and then dried for overnight. The mixture includes internal standard of 1,4-dichlorobenzene and bromobenzene, the as-obtained reacted solution as well as absolute ethanol was analyzed quantitatively by gas chromatography (GC) with a HP–5 ms capillary column (30 m, DF = 0.25 mm, 0.25 mm i.d.). The recycle performance was investigated under the same reaction conditions, however, the recycled catalyst was obtained via reannealing reacted catalyst at the same temperature.

3. Results and discussion

S–CoNC was prepared through a one-pot method as illustrated in Scheme 1. Cobalt nitrate hexahydrate and 1,10-phenanthroline (mole ratio of 1:2) were dissolved into absolute ethanol by sonicating to form homogeneous solution. There was a large amount of yellow precipitate $(Co(Phen)_2^{2+})$ after a period of stirring. KSCN has strong complexing ability besides rich nitrogen and sulfur. The yellow precipitate was immediately transformed to pink precipitate upon adding KSCN into this solution. It was noteworthy that the generated pink precipitate was $(Co(Phen)_2(SCN)_2)$. The final pink product after filtration and drying was pyrolyzed at 800 °C for 2 h to obtain S–CoNC.

The crystallographic phases of samples were investigated by X-ray diffraction (XRD), as shown in Fig. 1a. According to the diffractogram of S–CoNC, there is a broad peak ascribed to graphite-type carbon at *ca.* 25°, while many sharp peaks appeared at 29.9°, 31.1°, 36.2°, 39.5°, 47.6°, and 54.6° are indexed to the (311), (222), (400), (331), (511), and (531) planes of hexagonal Co_4S_3 (JCPDS No. 02-1338), respectively, which suggest that cobalt has been sulfured via a simple heating treatment. Moreover, the pattern of S–CoNC also gives two weak peaks
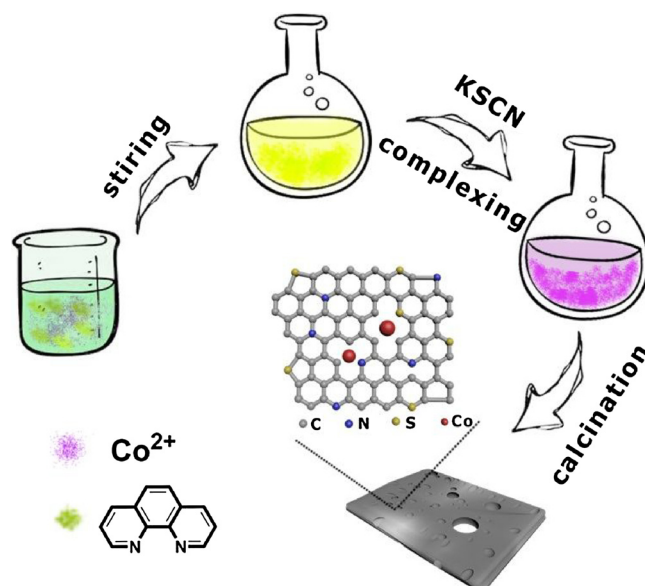
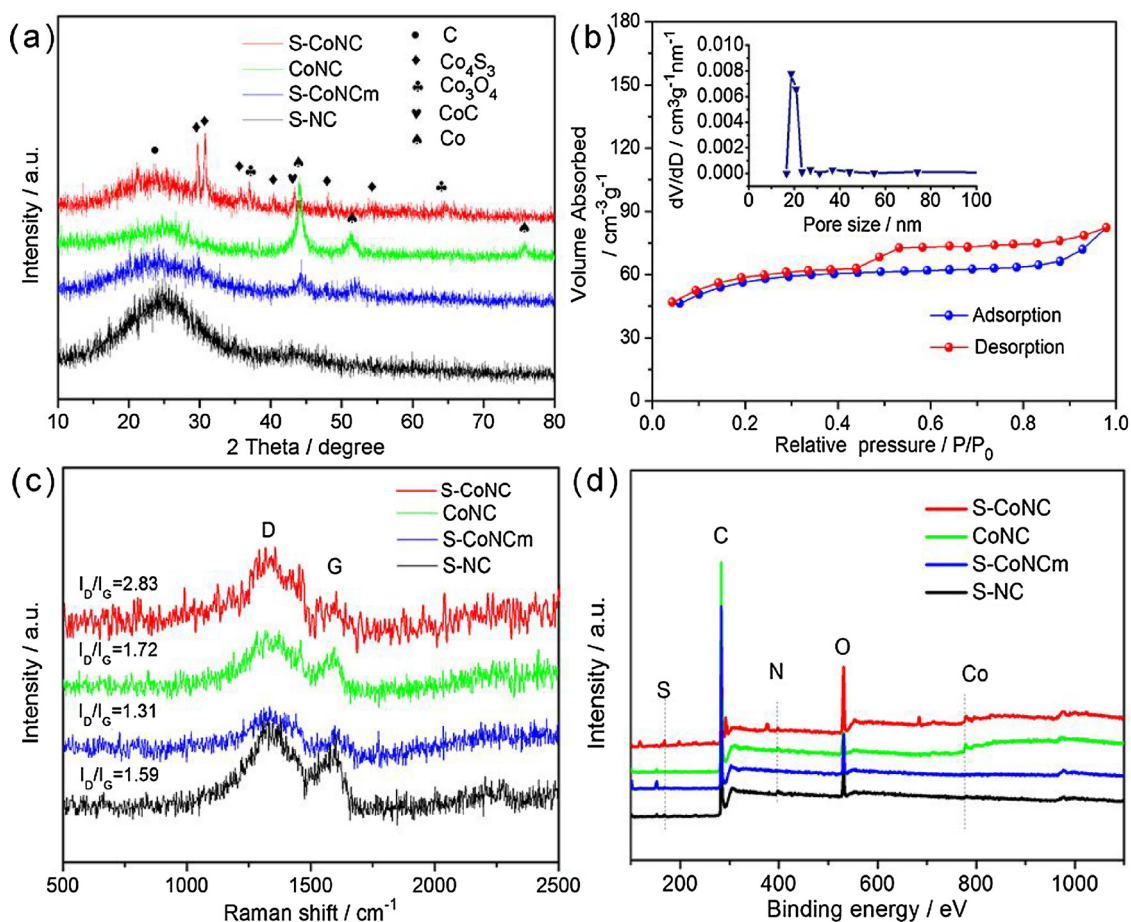**Scheme 1.** Scheme illustration of preparation of S–CoNC.

Fig. 1. (a) XRD patterns of samples. (b) Nitrogen adsorption–desorption isotherm with pore size distribution (insert) of S–CoNC. (c) Raman spectrum of samples. (d) XPS survey spectrum of samples.

Table 1
Textural properties of as-prepared samples.

Sample	Specific surface area (m^2/g)	Pore Volume (cm^3/g)	Pore diameter (nm)
S–CoNC-700	144	0.08	20.0
S–CoNC	183	0.12	19.9
S–CoNC-900	209	0.13	20.0
CoNC	106	0.09	18.6
S–NC	793	0.48	19.8
S–CoNCm	118	0.08	3.7

at 36.8° and 65.2° corresponding to cubic Co_3O_4 (JCPDS No. 43-1003). And the characteristic peak of CoC is also observed at 43.5°. In order to characterize the specific surface area and porosity of S–CoNC, nitrogen adsorption–desorption isotherm was measured and calculated by Brunauer–Emmett–Teller (BET) and Barrett–Joyner–Hallender (BJH) methods (Fig. 1b) [24,25]. The isotherm shows a type IV with H4 hysteresis loop in $P/P_0 = 0.4–0.98$, from which the specific surface area is estimated to be $183\,m^2/g$ and the pore size distributions suggest the formation of mesopores with 19.9 nm (Table 1). The findings are even larger than CoNC/CNT and CoNC/CB derived from the pyrolysis of 1,10-phenanthroline precursor reported by Yu group [26]. However, S–CoNC was prepared without support and just with the assistant of KSCN, thus, it can speculate that KSCN is conductive to increasing specific surface area and broadening pore size of sample. In addition, the structural information about S–CoNC was obtained from Raman spectrum (Fig. 1c), the D and G bands are located at around 1350 and $1590\,cm^{-1}$, respectively. Obviously, there are strong D band peak and weak G band peak in this spectrum, and the D band is associated with

structural defects [27]. It is noteworthy that the D to G band intensity ratio (I_D/I_G) that is an indicator of the defects level is up to 2.83, which is far higher than some values such as 0.78, 0.91 and so on, reported by previous work [28,29]. The high defect ratio is thought to produce more structure defect than other samples, which are beneficial to enhancing catalytic performance of samples [30].

The morphology and microstructure of sample was characterized by scanning electron microscopy (SEM) and transmission electron microscopy (TEM). Fig. 2a shows bulk solid materials with relatively smooth surface and rough cross section. There are many small holes in the low magnification TEM image (Fig. 2b), which originate from the effect of pore-forming agent of KSCN and account for higher specific surface area, in consistent with the results of nitrogen sorption. The high resolution TEM image reveals that the lattice spacing (*d*) of cobalt species are 0.28 and 0.23 nm, corresponding to the (222) plane of hexagonal Co_4S_3 and cubic Co_3O_4 (Fig. 2c), respectively, further confirming cobalt is sulfured. It is worth noting that there are no visible cobalt nanoparticles in whole carbonaceous material, demonstrating that cobalt nanoparticles are fine and uniform dispersibility, which are owing to the growth of metal nanoparticles inhibited by nitrogen and sulfur heteroatoms [31,32], demonstrating by the elemental mapping images (Fig. S1). The TEM image of CoNC presents large metal particles and irregular carbonaceous matrix (Fig. 2d), it further confirms that doping of sulfur is in favor of limit of the aggregation of metal particles. Fig. 2e illustrates that metal particles are completely removed by etching with acidic solution. And the S–CoNCm from mercapto acetic acid shows irregular carbonaceous matrix without obvious metal particles (Fig. 2f).

The chemical compositions and states of S–CoNC were carried out in X-ray photoelectron spectroscopy (XPS). The main elements in S–CoNC
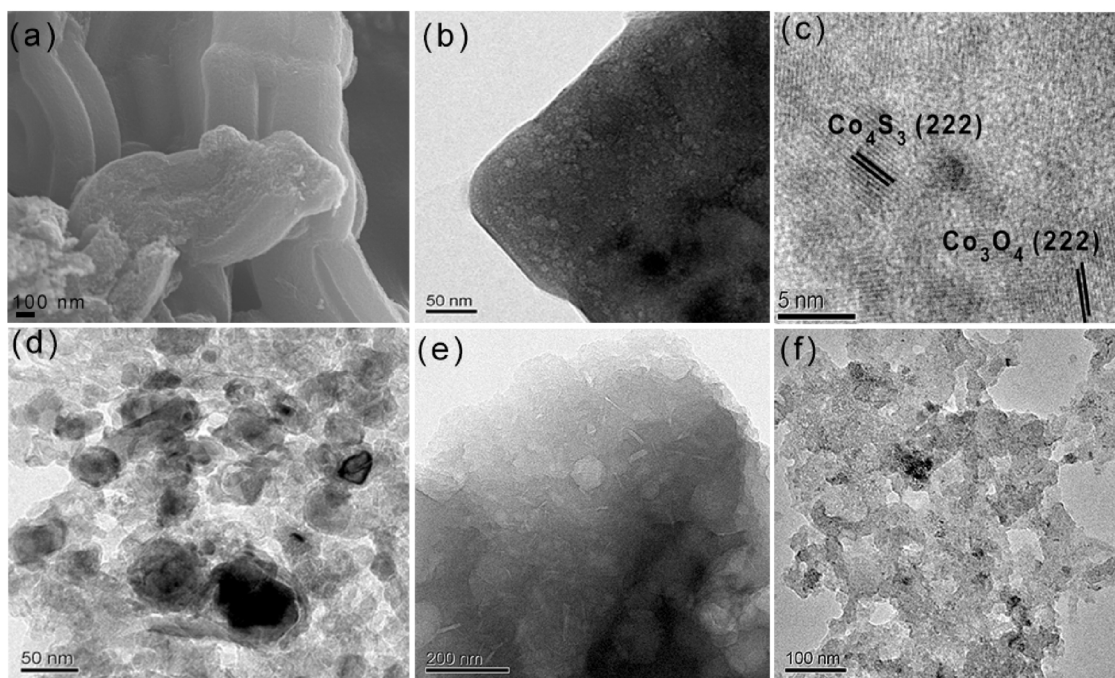
Fig. 2. (a–c) are SEM, TEM, and HRTEM images of S–CoNC, respectively. (d–f) are TEM images of CoNC, S–NC, and S–CoNCm.
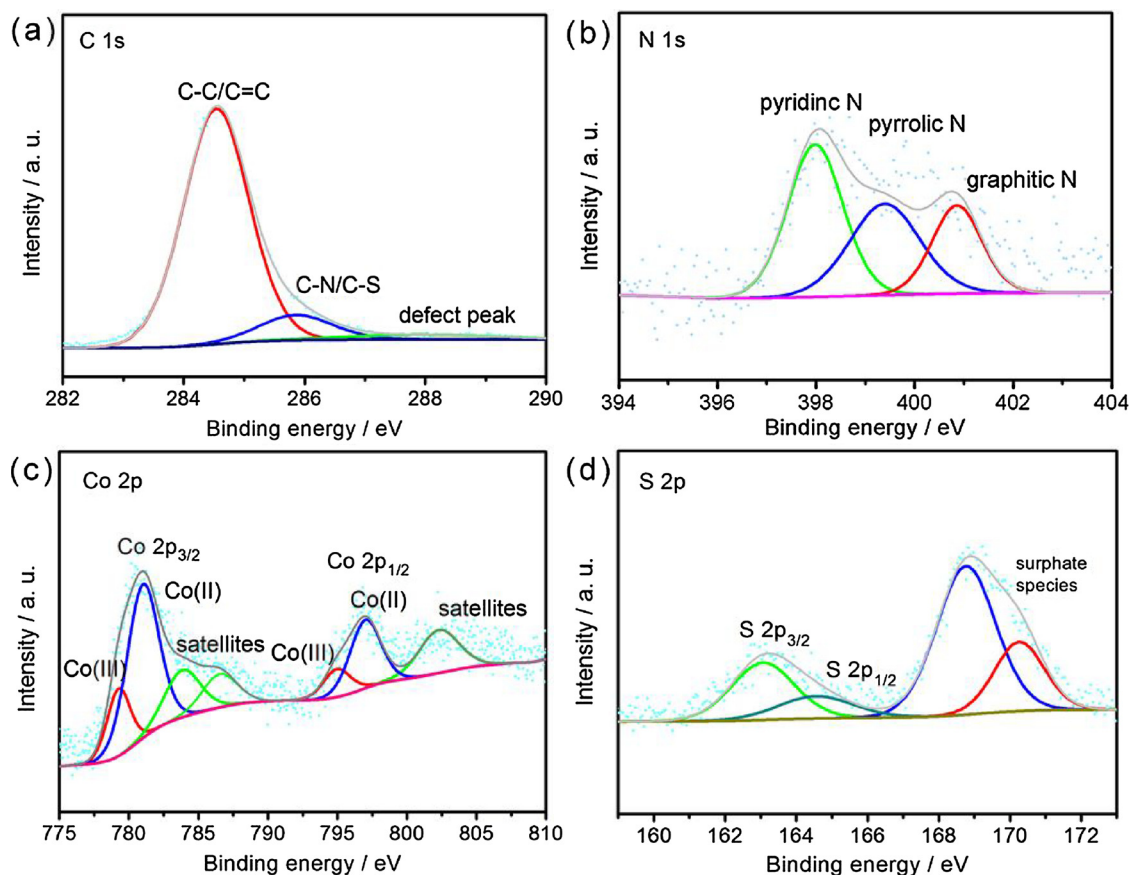

Fig. 3. High resolution (a) C 1s, (b) N1s, (c) Co 2p, and (d) S 2p XPS spectrum of S–CoNC, respectively.

are C, N, O, Co, and S seen from the survey spectrum (Fig. 1d), further confirming the successful incorporation of sulfur atom into framework. Fig. 3a shows the fitted high resolution XPS spectrum of C 1s peak. The peaks appeared at 284.5 and eV 285.7 are indexed to the C−C or C≡C graphite bonds and C−S or C−N bonds, respectively. A weak 288.2 eV

peak is attributed to the defects and functional groups like C−N, C−O, and O−C−O [33], which is in consistent with the Raman results [29]. The broad N 1s spectrum is deconvoluted into three peaks with binding energies at 398.0, 399.4, and 400.8 eV, corresponding to pyridinic N, pyrrolic N, and graphitic N, respectively (Fig. 3b). The content of

Table 2
Catalytic performance for oxidation of ethylbenzene by S–CoNC.[a]

Entry	Catalyst	Conversion (%)	Selectivity (%)		
			AcPO	PEA	BA
1	Blank	6	60	35	5
2	Co(Phen)$_2$(SCN)$_2$	33	79	17	4
3	S–CoNC-700	46	76	24	–
4	S–CoNC	62	91	9	–
5	S–CoNC-900	37	72	28	–
6	CoNC	8	78	22	–
7	S–NC	7	75	25	–
8	S–Co	39	80	20	–
9	S–CoNCm	12	80	20	–
10	S–CoNC[b]	79	90	10	–
11	S–CoNC[c]	82	88	12	–
12	S–CoNC-R[d]	8	87	13	–
13	S–CoNC-R-C1[e]	65	92	8	–
14	S–CoNC-R-C2[f]	61	91	9	–
15	S–CoNC[g]	–	–	–	–
16	S–CoNC[h]	15	81	19	–

[a] Reaction conditions: 120 °C, 5 h, 10 mL of ethylbenzene (82 mmol), 30 mg of catalyst, and 0.8 MPa of O$_2$, acetophenone (AcPO), phenethyl alcohol (PEA), and benzaldehyde (BA).

[b] Reaction time was prolonged to 10 h based on other same conditions.

[c] Reaction time was prolonged to 20 h based on other same conditions.

[d] The second reaction at the same conditions after the first reaction.

[e] The catalyst reacted for 1 time was reannealed at the same temperature.

[f] The catalyst was annealed for another 1 time based on the former conditions of e.

[g] Reaction conditions are consistent with this work beside adding butylated hydroxytoluene (BHT) (1 mL).

[h] 1 mmol of fluobenzene was added based on the same conditions.

pyridinic N is more than that of pyrrolic N and graphitic N, and pyridinic N which locates at the defect sites in the basal plane and is bonded to two adjacent carbon atoms provides highly active sites due to lower adsorption energy [34]. The Co 2p at 780.9 and 796.9 eV can be divided into Co 2p$_{3/2}$ and Co 2p$_{1/2}$, respectively, which are fitted into Co(III), Co(II), and satellites peaks (Fig. 3c). A high resolution of S 2p spectrum mainly shows three different peaks (Fig. 3d). The peaks at 163.2 eV of S 2p$_{3/2}$ and 164.6 eV of S 2p$_{1/2}$ are consistent with reported literature and assigned to −C−S−C− and −C≡S− bonds [30,35]. The other peaks belong to SO$_x$ groups with chemically inactive and occur at the edge of the carbon skeleton, meanwhile, the formation of SO$_x$ groups can be proved by the O 1s (Fig. S2). It is reported that the components at 163.2 eV are corresponding to metal–sulfur bonds [29].

Sulfur and nitrogen-doped metal carbon catalysts have been extensively researched, but there are few reports in heterogeneous catalysis. The oxidation of ethylbenzene with solvent-free and O$_2$ as oxidant was probed as the model reaction. It is known that Co/N-ligands complexes (especially Co/phthalocyanines) have catalytic performance for some catalytic reactions [36,37], so the catalytic activity of Co (Phen)$_2$(SCN)$_2$ was tested (Table 2, entry 2). The influence of pyrolysis temperature before studying the reaction system was investigated. The S–CoNC pyrolyzed at 800 °C shows the highest conversion of ethylbenzene (62%) and selectivity of AcPO (91%) compared with that of the catalysts pyrolyzed at 700 and 900 °C (Table 2, entries 3–5), demonstrating that 800 °C is the best temperature for preparing catalyst. The blank testing (without catalyst) gives extremely low catalytic activity in this system (Table 2, entry 1). In order to clearly study the effect of catalyst compositions for catalytic performance, some control experiments were tested (Table 2, entries 6–9). It is remarkable that there is poor catalytic performance in CoNC, S–NC, and S–CoNCm. The conversion of ethylbenzene is only around 10% and the selectivity of AcPO is also lower than 80%, which is obviously far lower than S–CoNC at the same reaction system. Moreover, the reaction time was prolonged

to 10 h and 20 h to take full advantage of the high active catalyst (Table 2, entries 10 and 11). Ethylbenzene conversion of 79% is achieved as reaction time is prolonged to 10 h, and it is up to 82% for 20 h. S–CoNC is of higher catalytic performance under similar reaction conditions than some reported catalysts (Table S1), as we know, it is so far the highest conversion rate of ethylbenzene under solvent-free and O$_2$ as oxidant. Unfortunately, the selectivity of AcPO is not further improved.

In order to thoroughly investigate the active sites in the reaction system, some detailed discussion was conducted. As shown in Fig. 1a, there are only metallic Co peaks in CoNC and S–CoNCm besides graphite-type carbon peak in XRD patterns, and the catalytic performance of CoNC, S–CoNCm and S–NC is far lower than S–CoNC, suggesting that Co$_4$S$_3$ may be the active site rather than metallic Co in the reaction system. Remarkably, no cobalt sulfides are detected in S–CoNCm derived from the pyrolysis of mercapto acetic acid, demonstrating that KSCN with strong complexing ability has an important role in the preparation of high performance samples. These samples have high specific surface area and similar pore size besides S–CoNCm, demonstrating that KSCN is used as a pore-forming agent in the process of preparing sample (Table 1). According to the Raman spectrum (Fig. 1c), the I$_D$/I$_G$ ratio of S–CoNC (2.83) is significantly larger than that of other samples (1.72, 1.59, and 1.31), indicating that S–CoNC possesses more defects than other samples, which are beneficial to enhancing catalytic performance of samples [30]. It is also proven that the defect of carbon based materials is not only improved by doping heteroatoms, but also linked with the connection between metal and heteroatom. Thus, we propose that Co$_4$S$_3$ may cause more defects in samples. And the doped sulfur is beneficial for inhibiting the growth of metal particles as demonstrated by Fig. 2. A large number of SO$_x$ groups with chemical inactivity and few −C−S−C and −C≡S− structures are presented in the S 2p of S−NC and S−CoNCm (Fig. S3), suggesting that there are hardly any metal sulfides in these samples. The elements analysis of samples is summarized in Table S2. To sum up, Co$_4$S$_3$ should be the catalytic active site for the aerobic oxidation of ethylbenzene.

Stability is an important parameter for judging the performance of catalyst. Unexpectedly, an extremely low conversion was obtained after the second reaction (Table 2, entry 12). There is no apparent agglomeration in the reacted catalyst (Fig. S5). It is amazing that S–CoNC recovers the conversion and selectivity after annealing the reacted catalyst at the same temperature (Table 2, entries 13 and 14). The reacted catalyst (S–CoNC-R) and reannealed catalyst (S–CoNC-R-C) were characterized in order to investigate the differences. The XRD patterns show that there are many undesired peaks in S–CoNC-R, but there are almost Co$_4$S$_3$ peaks in S–CoNC-R-C (Fig. 4), suggesting that Co$_4$S$_3$ can be reformed through high temperature anneal, and proving the importance of Co$_4$S$_3$ in the reaction system. Moreover, S–CoNC-R has no
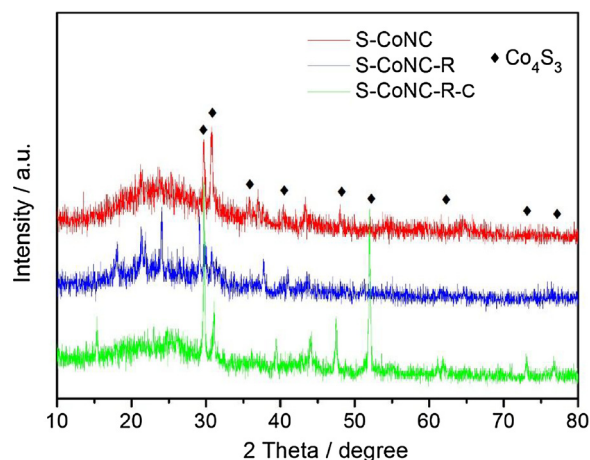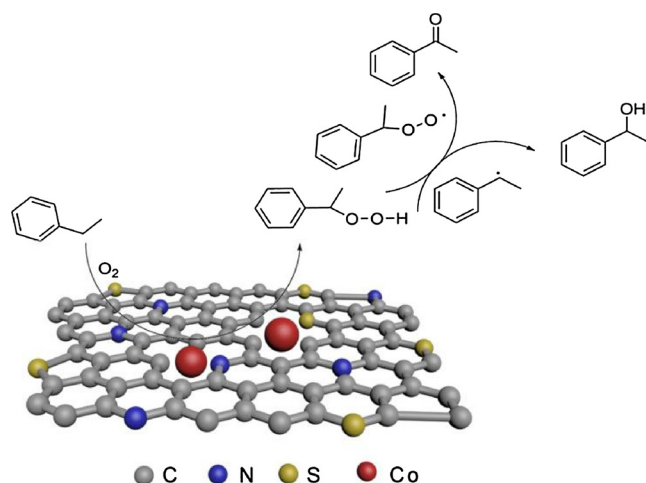

Fig. 4. XRD patterns of S–CoNC-R and S–CoNC-R-C.

Fig. 5. Proposed reaction promotion mechanism by S–CoNC.

active sulfur species including −C−S−C and −C=S− (Fig. S3), instead of the existence of lots of inactive SO$_x$ groups. The reason for the high activity of S–CoNC-R-C is due to the presence of −C−S−C and −C=S− and reformed metal–sulfur bonds. Although the content of cobalt and sulfur of S–CoNC-R-C is lower than S–CoNC and other samples (Table S2), the catalytic performance has not been significantly affected, further demonstrating that Co$_4$S$_3$ is the active site. A large number of fluorine elements were detected in the XPS survey spectrum of S–CoNC-R (Fig. S4). The ethylbenzene oxidation reaction is free radical reaction demonstrated via the addition of radical scavenger of butylated hydroxytoluene (BHT) in reaction system and reported by previous report and our work (Table 2, entry 15) [5,38,39]. 1-phenyl-ethylhydroperoxide (PEHP) is an important intermediate compound for production of AcPO and PEA and the main chain propagator in this reaction pathway,

which originates from the oxidation of ethylbenzene with O$_2$ in a free radical way (Fig. 5). The fluorine, an electron-withdrawing functional group, maybe absorb free radical electrons to decrease catalytic performance (Table 2, entry 16).

To explore the scope of S–CoNC based on above results, solvent-free and aerobic oxidation of other hydrocarbons were researched under the optimized reaction conditions. Table 3 shows that S–CoNC has superior catalytic activity for a wide range of substrate. 4-ethyltoluene containing electron-donating functional group affords higher conversion than p-bromoethylbenzene with electron-withdrawing functional group within 5 h (Table 3, entries 1 and 2). Analogous to ethylbenzene, S–CoNC is also presenting excellent catalytic activity for n-propylbenzene and cumene (Table 3, entries 3 and 4). The catalyst also functions in the oxidation of diphenylmethane with a moderate conversion, possibly because of the steric hindrance (Table 3, entry 5). The oxidation of tetralin and indane to corresponding products is an important application in industry [40,41]. Catalyzed by S–CoNC, tetralin and indane afford superior conversion and selectivity to main products (Table 3, entries 6 and 7). All of the above results suggest that S–CoNC has excellent catalytic performance for various hydrocarbons under O$_2$ and solvent-free conditions.

4. Conclusion

In summary, we have successfully prepared sulfur and nitrogen-doped porous cobalt carbon catalyst through a simple but efficient one-pot method, in which KSCN is not only as sulfur source, but also as complexing agent. There is high specific surface area under the help of KSCN, which is significantly higher than other materials with support or pore-forming agent. The as-prepared catalyst is of higher defect ratio (up to 2.83) than other controlled catalysts. The catalyst has excellent catalytic performance for oxidation of hydrocarbons under solvent-free and O$_2$ as oxidant, especially for ethylbenzene, 82% is so far the highest

Table 3
Aerobic oxidation of hydrocarbons catalyzed by S–CoNC.[a]

Entry	Substrate	Product		Con. [%]	Sel. [%]
1				78	88
2				37	86
3				52	70
4				74	63, 37
5				31	95
6				69	75, 25
7				60	60, 40

[a] Reaction conditions: hydrocarbons 82 mmol, catalyst 30 mg, O$_2$ 0.8 MPa, and 5 h.

conversion rate under the reaction conditions, the reason of high activity is owing to the active site of Co_4S_3 and structure defect. The new catalyst not only perfects the application of sulfur and nitrogen-doped carbon catalysts, but also provides a new thought for developing novel sulfur doped materials.

Conflicts of interest

The authors declare no competing financial interest.

Acknowledgements

Appendix A. Supplementary data

Supplementary data associated with this article can be found, in the online version, at http://dx.doi.org/10.1016/j.mcat.2018.05.031.

References

[1] J. Fan, Y. Dai, Y. Li, N. Zheng, J. Guo, X. Yan, G.D. Stucky, J. Am. Chem. Soc. 131 (2009) 15568–15569.
[2] J. Zhang, X. Liu, R. Blume, A.H. Zhang, R. Schlögl, D.S. Su, Science 322 (2008) 73–77.
[3] M. Jafarpour, A. Rezaeifard, V. Yasinzadeh, H. Kargar, RSC Adv. 5 (2015) 38460–38469.
[4] F.Z. Su, Y.M. Liu, L.C. Wang, Y. Cao, H.Y. He, K.N. Fan, Angew. Chem. 120 (2008) 340–343.
[5] X. Lin, Z. Nie, L. Zhang, S. Mei, Y. Chen, B. Zhang, R. Zhu, Z. Liu, Green Chem. 19 (2017) 2164–2173.
[6] X. Cai, Q. Wang, Y. Liu, J. Xie, Z. Long, Y. Zhou, J. Wang, ACS Sustain. Chem. Eng. 4 (2016) 4986–4996.
[7] S. Shi, C. Chen, M. Wang, J. Ma, J. Gao, J. Xu, Catal. Sci. Technol. 4 (2014) 3606–3610.
[8] Y. Gao, G. Hu, J. Zhong, Z. Shi, Y. Zhu, D.S. Su, J. Wang, X. Bao, D. Ma, Angew. Chem. Int. Ed. 52 (2013) 2109–2113.
[9] R. Kothandaraman, V. Nallathambi, K. Artyushkova, S.C. Barton, Appl. Catal. B 92 (2009) 209–216.
[10] I. Matanovic, S. Babanova, A. Perry III, A. Serov, K. Artyushkova, P. Atanassov, Phys. Chem. Chem. Phys. 17 (2015) 13235–13244.
[11] S. Guo, P. Yuan, J. Zhang, P. Jin, H. Sun, K. Lei, X. Pang, Q. Xu, F. Cheng, Chem. Commun. 53 (2017) 9862–9865.
[12] L. He, F. Weniger, H. Neumann, M. Beller, Angew. Chem. Int. Ed. 55 (2016) 12582–12594.
[13] Y. Cao, S. Mao, M. Li, Y. Chen, Y. Wang, ACS Catal. 7 (2017) 8090–8112.
[14] S. Kumar, A. Baruah, S. Tonda, B. Kumar, V. Shanker, B. Sreedhar, Nanoscale 6 (2014) 4830–4842.
[15] M. Li, F. Xu, H. Li, Y. Wang, Catal. Sci. Technol. 6 (2016) 3670–3693.
[16] S.A. Wohlgemuth, R.J. White, M.G. Willinger, M.M. Titirici, M. Antonietti, Green Chem. 14 (2012) 1515–1523.
[17] S. Wang, L. Zhang, Z. Xia, A. Roy, D. Wook Chang, J.B. Baek, L. Dai, Angew. Chem. Int. Ed. 51 (2012) 4209–4212.
[18] Z. Yao, H. Nie, Z. Yang, X. Zhou, Z. Liu, S. Huang, Chem. Commun. 48 (2012) 1027–1029.
[19] D.H. Kwak, S.B. Han, Y.W. Lee, H.S. Park, I.A. Choi, K.B. Ma, M.C. Kim, S.J. Kim, D.H. Kim, J.I. Sohn, K.W. Park, Appl. Catal. B 203 (2017) 889–898.
[20] P. Liang, C. Zhang, X. Duan, H. Sun, S. Liu, M.O. Tade, S. Wang, ACS Sustain. Chem. Eng. 5 (2017) 2693–2701.
[21] W. Zhong, H. Liu, C. Bai, S. Liao, Y. Li, ACS Catal. 5 (2015) 1850–1856.
[22] P. Chen, T. Zhou, L. Xing, K. Xu, Y. Tong, H. Xie, L. Zhang, W. Yan, W. Chu, C. Wu, Y. Xie, Angew. Chem. Int. Ed. 56 (2017) 610–614.
[23] A.A. Schilt, K. Fritsch, J. Inorg, Nucl. Chem. 28 (1996) 2677–2683.
[24] S. Brunauer, P.H. Emmett, E. Teller, J. Am. Chem. Soc. 60 (1938) 309–319.
[25] E.P. Barrett, L.G. Joyner, P.H. Halenda, J. Am. Chem. Soc. 73 (1951) 373–380.
[26] T. Cheng, H. Yu, F. Peng, H. Wang, B. Zhang, D. Su, Catal. Sci. Technol. 6 (2016) 1007–1015.
[27] C.V. Rao, C.R. Cabrera, Y. Ishikawa, J. Phys. Chem. Lett. 1 (2010) 2622–2627.
[28] P.P. Sharma, J. Wu, R.M. Yadav, M. Liu, C.J. Wright, C.S. Tiwary, B.I. Yakobson, J. Lou, P.M. Ajayan, X.D. Zhou, Angew. Chem. 127 (2015) 13905–13909.
[29] G. He, M. Qiao, W. Li, Y. Lu, T. Zhao, R. Zou, B. Li, J.A. Darr, J. Hu, M.M. Titirici, I.P. Parkin, Adv. Sci. 4 (2017) 1600214.
[30] Y. Ito, W. Cong, T. Fujita, Z. Tang, M. Chen, Angew. Chem. 127 (2015) 2159–2164.
[31] Y. Cao, M. Tang, M. Li, J. Deng, F. Xu, L. Xie, Y. Wang, ACS Sustain. Chem. Eng. 5 (2017) 9894–9902.
[32] Y. Su, Y. Zhu, H. Jiang, J. Shen, X. Yang, W. Zou, J. Chen, C. Li, Nanoscale 6 (2014) 15080–15089.
[33] Y. Gao, H. Zhao, D. Chen, C. Chen, F. Ciucci, Carbon 94 (2015) 1028–1036.
[34] A.G. Kannan, J. Zhao, S.G. Jo, Y.S. Kang, D.W. Kim, J. Mater. Chem. A 2 (2014) 12232–12239.
[35] Z. Luo, C. Tan, X. Zhang, J. Chen, X. Cao, B. Li, Y. Zong, L. Huang, X. Huang, L. Wang, W. Huang, H. Zhang, Small 12 (2016) 5920–5926.
[36] J. Manassen, A. Bar-Ilan, J. Catal. 17 (1970) 86–92.
[37] C. Guo, Q. Peng, Q. Liu, G. Jiang, J. Mol. Catal. A 192 (2003) 295–302.
[38] J. Luo, F. Peng, H. Yu, H. Wang, W. Zheng, ChemCatChem 5 (2013) 1578–1586.
[39] I. Hermans, J. Peeters, P.A. Jacobs, J. Org. Chem. 72 (2007) 3057–3064.
[40] I. Llabrés, F.X. Xamena, O. Casanova, T.R. Galiasso, H. Garcia, A. Corma, J. Catal. 255 (2008) 220–227.
[41] A.C. Estrada, M.M.Q. Simões, I.C.M.S. Santos, M.G.P.M.S. Neves, A.M.S. Silva, J.A.S. Cavaleiro, A.M.V. Cavaleiro, Appl. Catal. A 366 (2009) 275–281.